# Structural Basis for the Heterotropic and Homotropic Interactions of Invertebrate Giant Hemoglobin[†,‡]

Nobutaka Numoto,[§,||,⊥] Taro Nakagawa,[||,@,#] Akiko Kita,[+] Yuichi Sasayama,[●] Yoshihiro Fukumori,*[,@,○] and Kunio Miki*[,§,○,◇]

*Department of Chemistry, Graduate School of Science, Kyoto University, Sakyo-ku, Kyoto 606-8502, Japan, Department of Life Science, Graduate School of Natural Science and Technology, Kanazawa University, Kanazawa, Ishikawa 920-1192, Japan, Research Reactor Institute, Kyoto University, Kumatori, Osaka 590-0494, Japan, Division of Biodiversity, Noto Marine Laboratory, Institute of Nature and Environmental Technology, Kanazawa University, Uchiura, Ishikawa 927-0553, Japan, and RIKEN SPring-8 Center at Harima Institute, Koto 1-1-1, Sayo-cho, Sayo-gun, Hyogo 679-5148, Japan*

*Received July 5, 2008; Revised Manuscript Received September 2, 2008*

ABSTRACT: The oxygen binding properties of extracellular giant hemoglobins (Hbs) in some annelids exhibit features significantly different from those of vertebrate tetrameric Hbs. Annelid giant Hbs show cooperative oxygen binding properties in the presence of inorganic cations, while the cooperativities of vertebrate Hbs are enhanced by small organic anions or chloride ions. To elucidate the structural basis for the cation-mediated cooperative mechanisms of these giant Hbs, we determined the crystal structures of $Ca^{2+}$- and $Mg^{2+}$-bound Hbs from *Oligobrachia mashikoi* at 1.6 and 1.7 Å resolution, respectively. Both of the metal-bound structures were determined in the oxygenated state. Four $Ca^{2+}$-binding sites and one $Mg^{2+}$-binding site were identified in each tetramer subassembly. These cations are considered to stabilize the oxygenated form and increase affinity and cooperativity for oxygen binding, as almost all of the $Ca^{2+}$ and $Mg^{2+}$ cations were bound at the interface regions, forming either direct or hydrogen bond-mediated interactions with the neighboring subunits. A comparison of the structures of the oxygenated form and the partially unliganded form provides structural insight into proton-coupled cooperativity (Bohr effect) and ligand-induced transitions. Two histidine residues are assumed to be primarily associated with the Bohr effect. With regard to the ligand-induced cooperativity, a novel quaternary rotation mechanism is proposed to exist at the interface region of the dimer subassembly. Interactions among conserved residues Arg E10, His F3, Gln F7, and Val E11, together with the bending motion of the heme molecules, appear to be essential for quaternary rearrangement.

Mammalian tetrameric hemoglobin (Hb)[1] is an allosteric protein that has been extensively studied for a century, ever since cooperative properties were discovered in its oxygen equilibrium curve (*1*). In the 1960s through the early 1970s, the cooperativity of tetrameric Hb had been identified with good accuracy by the successfully determined three-dimensional structures of oxygenated Hb (oxyHb) and deoxygenated Hb (deoxyHb) (*2*), together with the theoretical Monod−Wyman−Changeux (MWC) model (*3*) for multisubunit allosteric proteins. The MWC model assumes that the molecule would assume two types of quaternary structure, a low-ligand affinity T state and a high-ligand affinity R state; no intermediate structure is permitted. Perutz's stereochemical mechanism based on the remarkable quaternary structural changes between oxyHb and deoxyHb is in good agreement with the R and T states of the MWC model, and this mechanism provides reasonable explanations for cooperative oxygen binding. The tetrameric Hb exhibits both homotropic interactions (e.g., ligand−ligand such as oxygen interactions) and heterotropic interactions observed between ligand and nonligand molecules. In the case of vertebrate Hb, the molecules involved in heterotropic interactions are protons

[†] This work was supported by a grant from the National Project on Protein Structural and Functional Analyses to K.M. and a Grant-in-Aid for Scientific Research on Priority Areas (16087205) to Y.F. from the Ministry of Education, Culture, Sports, Science, and Technology of Japan.

[‡] The coordinates have been deposited in the Protein Data Bank as entries 2ZS0 and 2ZS1.

* To whom correspondence should be addressed. K.M.: telephone, +81-75-753-4029; fax, +81-75-753-4032; e-mail, miki@kuchem.kyoto-u.ac.jp. Y.F.: telephone, +81-76-264-6231; fax, +81-76-264-6230; e-mail, fukumor@kenroku.kanazawa-u.ac.jp.

[§] Graduate School of Science, Kyoto University.

[||] These authors contributed equally to this work (performed research).

[⊥] Current address: Department of Life Science, Graduate School of Natural Science and Technology, Kanazawa University, Kanazawa, Ishikawa 920-1192, Japan.

[@] Graduate School of Natural Science and Technology, Kanazawa University.

[#] Current address: Research Center for Micro-Nano Technology, Hosei University, Koganei, Tokyo 184-0003, Japan.

[+] Research Reactor Institute, Kyoto University.

[●] Institute of Nature and Environmental Technology, Kanazawa University.

[○] These authors contributed equally to this work (designed research).

[◇] RIKEN SPring-8 Center at Harima Institute.

[1] Abbreviations: Hb, hemoglobin; oxyHb, oxygenated hemoglobin; deoxyHb, deoxygenated hemoglobin; BPG, 2,3-bisphosphoglycerate; IHP, inositol hexaphosphate; HBL, hexagonal bilayer; PEG, polyethylene glycol; Ca-oxyHb, $Ca^{2+}$-bound form as the oxygenated state; Mg-oxyHb, $Mg^{2+}$-bound form as the oxygenated state; met(A1-oxy)Hb, (A1-oxy A2-met B1-met B2-met) state hemoglobin; $P_{50}$, partial pressure of oxygen at half-saturation; $n$, Hill coefficient.

10.1021/bi8012609 CCC: $40.75 
Published on Web 10/04/2008

and $CO_2$ (via proton-coupled cooperativity, i.e., the Bohr effect) or small organic anions such as 2,3-bisphosphoglycerate (BPG), inositol hexaphosphate (IHP), and ATP. In addition, $Cl^-$ is known to be an effecter for heterotropic interactions in some vertebrate Hbs (*4*−*7*). The MWC/Perutz model is based on detailed structural analyses and has been assumed to provide an excellent illustration of the mechanism of cooperativity caused not only by homotropic interactions but also by heterotropic interactions, as heterotropic effectors preferably bind to the T-state Hb and stabilize the low-ligand affinity structure. More comprehensive studies of the cooperativity of tetrameric Hb are ongoing. Some heterotropic ligands that bind to the R-state Hb have been identified in the past 5 years (*8, 9*), and inclusive investigations of the oxygenation properties of Hb have led to the proposal of a novel extended allostery model (*10*).

In contrast to mammalian or vertebrate tetrameric Hb, invertebrate Hbs show remarkable varieties in terms of quaternary structure and oxygen binding properties (*11*−*14*). Two types of extracellular giant Hbs occur in some annelids. Earthworm *Lumbricus terrestris* has a 3600 kDa Hb designated as hexagonal bilayer (HBL) Hb, which also occurs in many other annelids. *Lumbricus* Hb shows moderate oxygen affinity and highly cooperative oxygen binding properties coupled with inorganic cations and protons (*15*). The heterotropic interactions involving inorganic cations are commonly observed features among annelid HBL Hbs (*12*). Cations and protons preferably bind to the R state and increase the ligand affinity of HBL Hbs; the heterotropic effectors in the annelid HBL Hbs differ markedly from those of vertebrate Hbs. Another giant Hb from an annelid is a 400 kDa Hb that occurs in some siboglinid polychaetes. *Oligobrachia mashikoi*, a frenulate beard worm, has a 400 kDa Hb (*16, 17*) composed of four globin subunits (A1, A2, B1, and B2) that form a 24-mer hollow-spherical structure (*18*). The oxygen binding properties of *Oligobrachia* Hb are qualitatively similar to those of annelid HBL Hbs. Both the oxygen affinity and cooperativity of *Oligobrachia* Hb are enhanced by the addition of $Ca^{2+}$ and/or $Mg^{2+}$, or by an increase in pH (*19*).

The crystal structures of the HBL Hbs (*20*−*22*) and 400 kDa Hbs (*18, 23*) have been reported recently, but the mechanisms of cooperativity via homotropic and heterotropic interactions are not well understood. Here, we report the crystal structures of the oxygenated state of $Ca^{2+}$- and $Mg^{2+}$-bound Hbs from *O. mashikoi* at 1.6 and 1.7 Å resolution, respectively. These structures provide insights into the allosteric mechanisms associated with divalent cations as heterotropic effectors in giant Hb. We also examined the mechanism of homotropic cooperativity in *Oligobrachia* Hb by comparing the high-resolution structures of the oxygenated form in this study to the partially unliganded structure reported previously at 1.95 Å resolution (*24*).

## MATERIALS AND METHODS

*Protein Preparation and Crystallization.* The siboglinid polychaete *O. mashikoi* was collected as described previously (*25*). The 400 kDa Hb was purified as reported previously (*17*), followed by an additional column chromatography step (*24*).

Crystals were obtained by the hanging-drop vapor diffusion method at 20 °C using equal volumes of a protein solution and a reservoir solution containing 10−11% (w/v) polyethylene glycol (PEG) 10000, 200 mM Tris-HCl (pH 8.0), and 10 mM $CaCl_2$ or $MgCl_2$. Crystals grew within 1 week, with maximum dimensions of 0.3 mm × 0.3 mm × 1.0 mm.

*Data Collection and Model Refinement.* Prior to data collection, the crystals were soaked for 2−4 h in a solution of 50 mM Bis-Tris propane, 15% (w/v) PEG 10000, 50 mM $CaCl_2$ or $MgCl_2$, and 20% (v/v) glycerol adjusted to pH 7.4 with NaOH, and the crystals were flash-frozen under a nitrogen gas stream at −183 °C. X-ray diffraction experiments were performed at beamlines BL38B1, BL41XU, BL44XU, and BL45XU at SPring-8. The data were processed and scaled using the HKL2000 package (*26*) and truncated with the CCP4 program suite (*27*). For further refinement, 5% of the reflections were set apart as a random test set to calculate the $R_{free}$ values.

The structure of *Oligobrachia* oxyHb [Protein Data Bank (PDB) entry 2D2M] was used as a search model for the molecular replacement method by MOLREP (*28*). Several cycles of manual model rebuilding [COOT (*29*)] and refinement [REFMAC5 (*27, 30*) and CNS (*31*)] were performed. After each cycle, $2F_o - F_c$ and $F_o - F_c$ electron density maps were calculated to check the fit of the model to the maps. Solvent molecules were placed by identification of peaks of $>3\sigma$ in the $F_o - F_c$ map and with a geometry suitable for hydrogen bonding. Metal ions were identified by the coordination geometry and distances to be expected in metal coordination groups in proteins (*32*). Contributions of the isoforms of the B1 subunit (B1b) were also taken into account, as was the case with the partially unliganded state of *Oligobrachia* Hb (*24*). To avoid undesired increases in the parameters, the 10 substituted residues of the B1b subunit were added to the model as pseudodouble conformations. The Ramachandran plots revealed that 94.4% of the residues were in the most favored regions, and the remainders of residues were in additionally and generously allowed regions in both the $Ca^{2+}$- and $Mg^{2+}$-bound structures. The statistics for data collection and refinement are summarized in Table 1. The figures were prepared with PYMOL (http://pymol.sourceforge.net/).

## RESULTS

*Overall Structure.* The overall structures of both $Ca^{2+}$- and $Mg^{2+}$-bound forms of *Oligobrachia* Hb have the same conformation as that of the previously reported oxygenated form (*Oligobrachia* oxyHb) (*18*), in which no metal ions were observed (Figure 1). The structures of the $Ca^{2+}$- and $Mg^{2+}$-bound forms can be superimposed onto that of *Oligobrachia* oxyHb with root-mean-square (rms) displacements of 0.71 Å (3438 Cα atoms) and 0.66 Å (3438 Cα atoms), respectively. The $Ca^{2+}$- and $Mg^{2+}$-bound forms also have the same conformation. These structures can be superimposed onto each other with a rms displacement of 0.20 Å (3444 Cα atoms).

The electron densities around the heme pocket of both metal-bound structures show clear peaks of heme ligand molecules at all four subunits in the asymmetric unit (Figure 2a and Figure S1 of the Supporting Information). Because

Table 1: Data Collection and Refinement Statistics[a]

| | Ca-oxyHb | Mg-oxyHb |
|---|---|---|
| **Data Collection** | | |
| wavelength (Å) | 1.0000 | 1.0000 |
| space group | *R*32 | *R*32 |
| unit cell parameters (Å) | | |
| *a* | 110.72 | 111.30 |
| *c* | 274.36 | 274.93 |
| resolution (Å) | 50−1.60 (1.66−1.60) | 50−1.70 (1.76−1.70) |
| no. of observations | 925175 | 471179 |
| no. of unique reflections | 85070 | 72136 |
| completeness (%) | 99.8 (100) | 99.8 (99.7) |
| average $I/\sigma(I)$ | 38.6 (6.0) | 29.6 (3.7) |
| redundancy | 10.9 (10.3) | 6.5 (5.2) |
| $R_{merge}$[b] (%) | 4.7 (37.0) | 5.3 (45.3) |
| **Refinement** | | |
| $R_{work}$[c] (%) | 17.1 | 18.0 |
| $R_{free}$[d] (%) | 19.8 | 20.7 |
| no. of atoms | | |
| protein | 4510 | 4502 |
| heme and oxygen | 180 | 180 |
| $Ca^{2+}$ | 4 | 0 |
| $Mg^{2+}$ | 0 | 1 |
| $Cl^-$ | 1 | 1 |
| glycerol | 12 | 36 |
| water | 743 | 643 |
| average *B* factor (Å$^2$) | | |
| protein | 23.3 | 28.1 |
| ligand/ion | 24.2 | 31.9 |
| water | 38.5 | 41.8 |
| rms deviation from ideal | | |
| bonds (Å) | 0.009 | 0.008 |
| angles (deg) | 1.1 | 1.1 |

[a] Values in parentheses are for the highest-resolution shell. [b] $R_{merge} = \sum\sum_i|I(h) - I(h)_i|/\sum\sum_i I(h)$, where $I(h)$ is the mean intensity after rejection. [c] $R_{work} = \sum|F_o - F_c|/\sum F_o|$, where $F_o$ is the observed structure factor amplitude and $F_c$ is the calculated structure factor amplitude. [d] $R_{free}$ is the same as *R* but was calculated using a random set containing 5% of the data that were excluded during refinement.

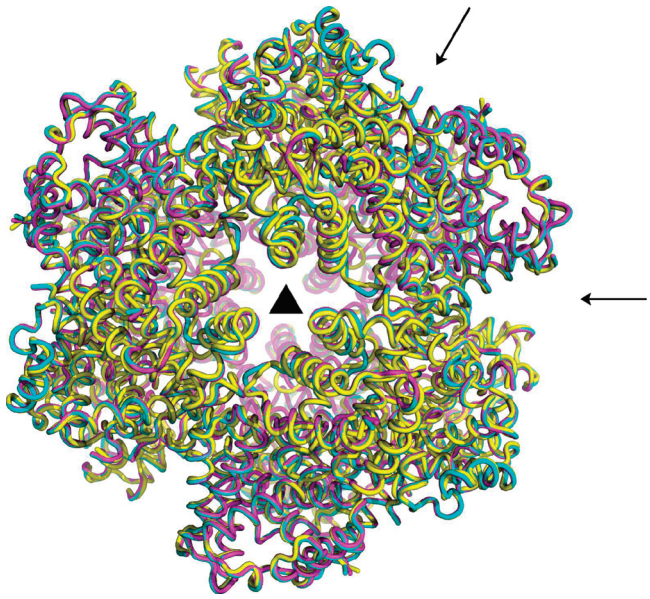

FIGURE 1: Overall structures of the $Ca^{2+}$-bound (magenta) and $Mg^{2+}$-bound (cyan) forms of *Oligobrachia* Hb superimposed onto that of *Oligobrachia* oxyHb (yellow, PDB entry 2D2M). The molecular 3- and 2-fold axes are indicated. All axes are parallel to the crystallographic symmetry axes.

the color of the metal-bound crystals was bright red, the structures were expected to exist primarily in the oxygenated state. The electron densities and refined occupancies, as well as the temperature factors of the ligands, are consistent with the fully coordinated features of the oxygen molecule at the A1 and B2 subunits. In contrast, the electron densities at the ligand sites of the A2 and B1 subunits are significantly and slightly weak, respectively. The following reasoning led us to refine the ligands at the latter two subunits as partially occupied oxygen molecules. Partially occupied diatomic oxygen molecules provide the best explanation for the observed electron densities. The temperature factors of the partially occupied oxygen molecules have been refined to reasonable values, and there is no apparent contradiction with the temperature factors associated with neighboring atoms.

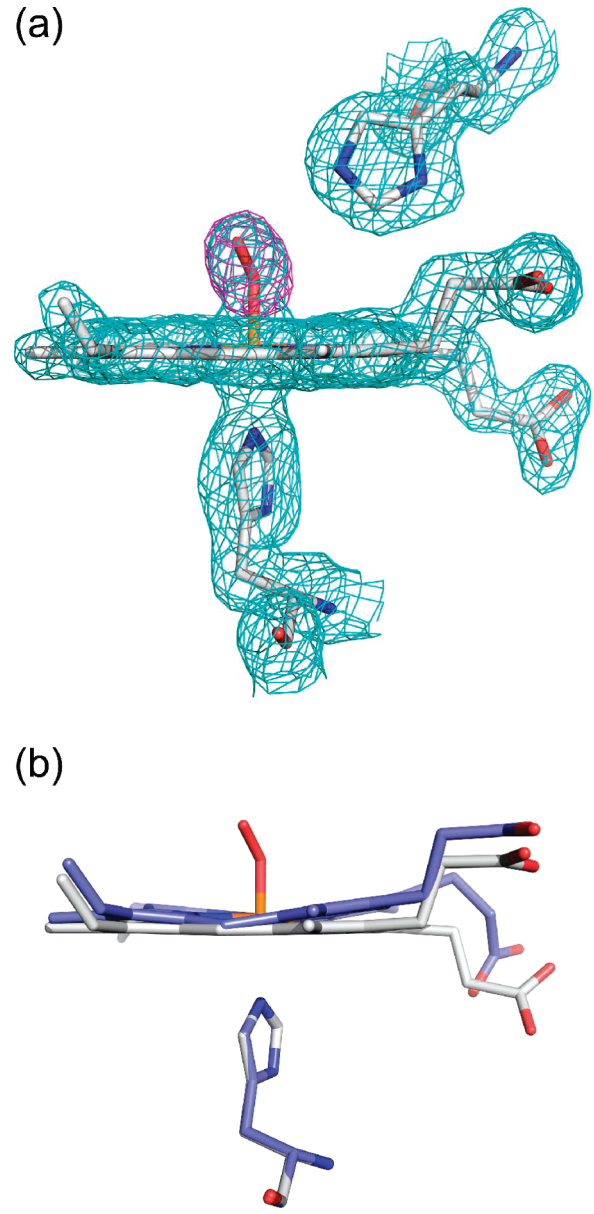


FIGURE 2: (a) $2F_o - F_c$ electron density map (cyan, contoured at $1.2\sigma$) and ligand-omitted $F_o - F_c$ map (magenta, contoured at $3.5\sigma$) around the ligand site of the B2 subunit of Ca-oxyHb. (b) Comparison of the heme geometry in the B2 subunit of Ca-oxyHb (white) with that of met(A1-oxy)Hb (blue). The models were superimposed by fitting of all atoms of the proximal histidines. Large deviations at the propionate groups were observed in all subunits, and the geometry of the oxygenated form was more planar than that of the unliganded form in all subunits. The complete diagrams of the electron density maps and geometries of the hemes at all subunits in both Ca- and Mg-oxyHb are presented in Figures S1 and S2 of the Supporting Information, respectively.

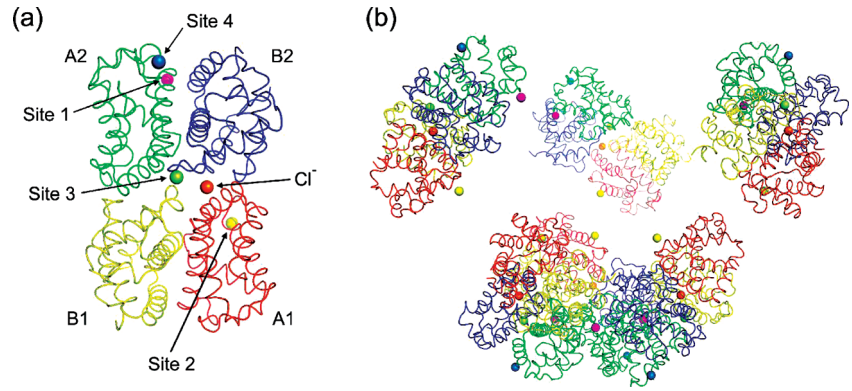


FIGURE 3: Positions of the $Ca^{2+}$ and $Cl^-$ ions in the crystal structure of Ca-oxyHb represented (a) as a tetramer subassembly (crystallographic asymmetric unit) and (b) as a split model of the whole 24-mer structure. Four $Ca^{2+}$ -binding sites (sites 1−4) and one $Cl^-$-binding site are indicated, and the positions of the ions are shown as spheres in different colors. Site 1 of $Ca^{2+}$ is equivalent to the $Mg^{2+}$-binding site of Mg-oxyHb. Subunits A1, A2, B1, and B2 are colored red, green, yellow, and blue, respectively.

There is another undeniable possibility that a fraction of a water molecule coordinated by the ferric heme has been present at both of the subunits, and this fraction serves as an alternative to partially occupied oxygen.

The following observations, in particular the detailed geometrical changes in the hemes, enabled us to evaluate the structural changes around the ligand-binding site: the high-resolution structures of the $Ca^{2+}$- and $Mg^{2+}$-bound forms in the oxygenated state (Ca-oxyHb and Mg-oxyHb, respectively) in this study and of the high-resolution structure of the partially unliganded met state (*24*), in which only the A1 subunit is oxygenated but the remaining three subunits are in the unliganded met state [met(A1-oxy)Hb]. Each heme in Ca- and Mg-oxyHb exhibits a geometry more planar than that of met(A1-oxy)Hb (Figure 2b and Figure S2 of the Supporting Information), as is also the case for oxygenated and deoxygenated human HbA (*33*).

*$Ca^{2+}$-Binding Sites.* Four $Ca^{2+}$-binding sites (sites 1−4) are identified in each tetramer subassembly (crystallographic asymmetric unit); the whole molecule has a total of 24 $Ca^{2+}$ ions in the crystal structure of Ca-oxyHb (Figure 3). Three of the four sites (sites 1−3) are located in the intersubunit regions, and site 4 is located at the surface of the molecule. The refinement assigned as fully occupied $Ca^{2+}$ ions results in the appearance of significant negative peaks in the $F_o - F_c$ difference Fourier maps. To achieve agreement with the calculated electron densities, the occupancies of all four $Ca^{2+}$ ions have been set to 0.7.

At site 1, the ligands of the $Ca^{2+}$ ion are the main chain carbonyl of Asp55 of the A2 subunit (A2 Asp55) and six waters, forming a heptacoordination (distorted pentagonal bipyramid) geometry (Figure 4a). The ligand waters form subsequent hydrogen bonds with the main chain carbonyls of A2′ (i.e., the neighboring A2 subunit in a dodecamer subassembly), at Arg122 and Phe124. It is noteworthy that site 1 is located near the zinc-binding site, which is also located at the interface between the A2 and A2′ subunits in the structure of 400 kDa coelomic Hb of *Riftia pachyptila* (tube worm) (*23*).

Site 2 is located at the interface between both A1 subunits of the dodecamer subassemblies. The $Ca^{2+}$ ion is coordinated by the main chain carbonyls of A1 Thr117 and A1′ Leu119, forming a hexacoordination (distorted octahedral) geometry (Figure 4b). Because site 2 is located near the crystallographic 2-fold symmetry axis, the $Ca^{2+}$ ion and ligand waters form a symmetrical cluster, including a water molecule at the special position. A cluster of $Ca^{2+}$ ions at the 3-fold symmetry axis have been reported in the structure of the collagen X NC1 domain trimer (*34*). The fully occupied metal cluster is buried in the trimer interface regions and contains a $Ca^{2+}$ ion at the special position, and the cluster is coordinated by all three subunits, significantly stabilizing the trimer assembly. In contrast, site 2 of Ca-oxyHb is situated on the inner surface of the hollow-spherical molecule and is exposed to solvent molecules. The partial occupancy of the $Ca^{2+}$ ion could be due to this environment.

Large structural differences are observed around site 3 in Ca-oxyHb and partially unliganded met(A1-oxy)Hb (Figure 4c). The $Ca^{2+}$ ion is coordinated by the side chains of A2 Asp78 and B2 Asp26, forming a heptacoordination geometry. Significant structural differences between Ca-oxyHb and met(A1-oxy)Hb were observed in the AB loop regions of all subunits. B2 Asp26, which is the third residue of the B helix in Ca-oxyHb and the first residue of the B helix in met(A1-oxy)Hb, is located near the AB loop region. The binding of the $Ca^{2+}$ ion at this site results in the stabilization of the oxygenated form by pushing both the B helix and the AB loop of the B2 subunit away from the A2 subunit, thereby prohibiting the formation of a tighter conformation in met(A1-oxy)Hb. The electron density map of A2 Asp78 indicated the presence of a small fraction of another rotamer reversed to the $Ca^{2+}$-binding site. The possibility of a double conformer supports the partial occupancy of the $Ca^{2+}$ ion at this site.

Site 4 is located on the molecular surface, and the $Ca^{2+}$ ion is coordinated by the main chain carbonyl of A2 Ser92 and the side chain of A2 Asp95, forming a heptacoordination geometry (Figure 4d). Although site 4 is near the region of contact of symmetry-related molecules, neither coordination nor hydrogen bond networks involving the $Ca^{2+}$ ion were observed between the two molecules at this site.

The dodecamer subassembly (half-molecule) of *Oligobrachia* Hb has many inner- and intersubunit disulfide bonds that preserve the dome-shaped structure. It has been demonstrated that met(A1-oxy)Hb dodecamer forms a tighter conformation than does oxyHb (*24*). Sites 1−3 are all placed at the interface regions of subunits in a molecule lacking intersubunit disulfide bonds. These findings suggest that bound $Ca^{2+}$ ions facilitate the stabilization of the oxygenated form of *Oligobrachia* Hb.

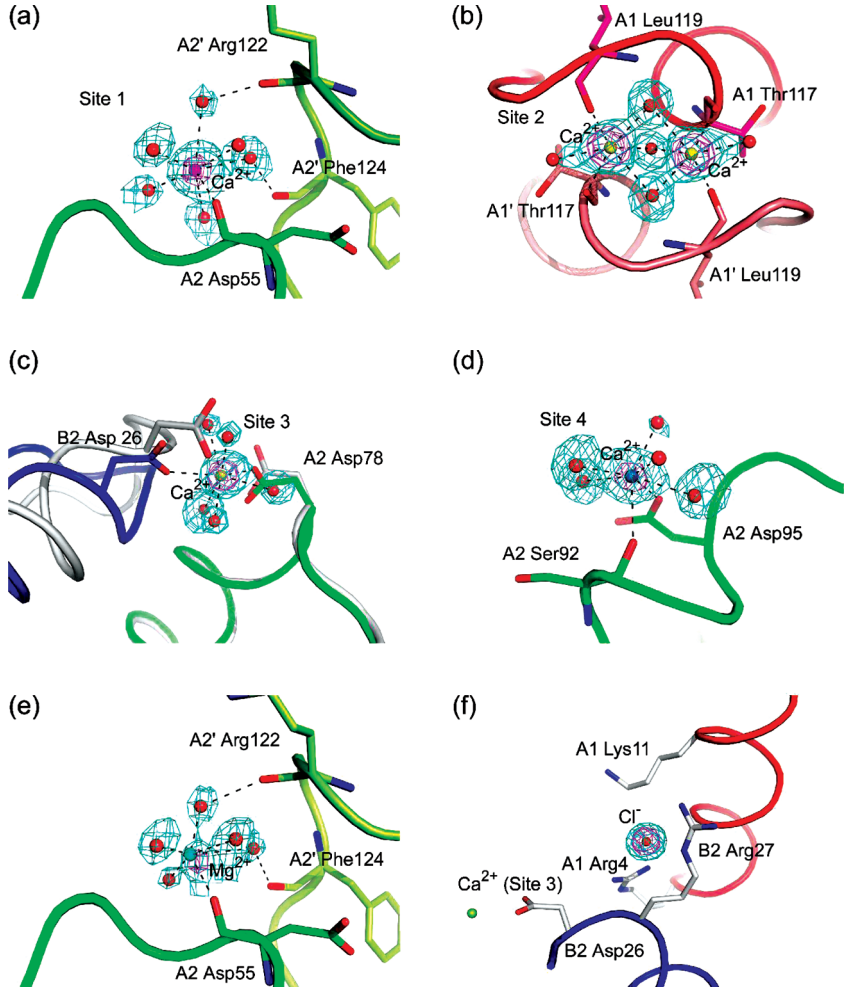


FIGURE 4: Close-ups of ion-binding sites. Sites 1−4 of the $Ca^{2+}$-binding sites are shown in panels a−d, respectively. The $2F_o - F_c$ maps (cyan, $1.2\sigma$) around $Ca^{2+}$ ions and ligand water molecules and the $Ca^{2+}$-omitted $F_o - F_c$ maps (magenta, $10\sigma$) are represented. The color schemes of the $Ca^{2+}$ ions and protein subunits are the same as that of Figure 3. Dashed lines indicate the coordination geometry of each metal ion. In panel c, the structure of met(A1-oxy)Hb (white) is superimposed on the A2 subunit of Ca-oxyHb. (e) The $Mg^{2+}$-binding site corresponds to site 1 of Ca-oxyHb. The $Mg^{2+}$ ion and the coordination atoms are represented as a cyan sphere and dashed lines, respectively. The maps were contoured at $1.2\sigma$ ($2F_o - F_c$ map) and $8\sigma$ ($F_o - F_c$ map). (f) $Cl^-$-binding site. The $Cl^-$ ion is represented as an orange sphere. Neighboring site 3 of the $Ca^{2+}$ ion is also shown. The maps were contoured at $1.2\sigma$ ($2F_o - F_c$ map) and $10\sigma$ ($F_o - F_c$ map).

*$Mg^{2+}$-Binding Site.* Only one $Mg^{2+}$-binding site (Figure 4e) that is identical to site 1 of Ca-oxyHb is found in the tetramer subassembly (i.e., the whole molecule has a total of six $Mg^{2+}$ ions in the crystal structure). As in the case of the $Ca^{2+}$ ion, the $Mg^{2+}$ ion is coordinated by the main chain carbonyl of A2 Asp55. There are five ligand waters forming a hexacoordination geometry. Hydrogen bonds between the ligand waters and main chain carbonyls of A2′ Arg122 and Phe124 are also observed. In Mg-oxyHb, an alternative, i.e., a water molecule, is found at the corresponding metal position at site 2 of Ca-oxyHb, and no solvent peaks are observed in the corresponding metal positions at site 3 or 4 of Ca-oxyHb.

*$Cl^-$-Binding Site.* A significant peak of electron density is found within the same solvent region in both Ca- and Mg-oxyHb. For the reasons given below, we have identified this peak as a chloride ion. The electron density is very high ($\sim 7.5\sigma$ in Ca-oxyHb), and when the model was refined to include a water molecule at this position, the value of the temperature factor was abnormally low. The atomic distances between the center of the peak and neighboring residues are significantly large for typical hydrogen bonds with solvent water. Positively charged residues, two arginines and a lysine, are located around the peak, and the side chains of the two arginines are coordinated (Figure 4f).

## DISCUSSION

*Heterotropic Interactions.* It has been reported that the presence of $Ca^{2+}$ and $Mg^{2+}$ ions significantly increases oxygen affinity and cooperativity in *Oligobrachia* Hb, with maximum $P_{50}$ and $n$ values of 0.19 mmHg and 2.5, respectively (*19*). Hill plots have revealed that the lower left end (oxygen affinity for the T state) is scarcely shifted but the upper right end (oxygen affinity for the R state) is shifted to the left in the presence of $Mg^{2+}$ ions, which indicates that $Mg^{2+}$ ions are bound during the late steps of oxygenation. In contrast, both the lower left and upper right ends are shifted to the left in the presence of $Ca^{2+}$ ions, indicating that $Ca^{2+}$ ions are bound sequentially during the early and late steps of oxygenation. These properties are confirmed by the structures of Ca- and Mg-oxyHb. All metal-binding sites, with the exception of site 4 of Ca-oxyHb, are located at the interfaces of subunits, rendering the oxygenated form sufficiently stabilized. The stabilization of the oxygenated form leads to the shifts to the left observed in the Hill plots.

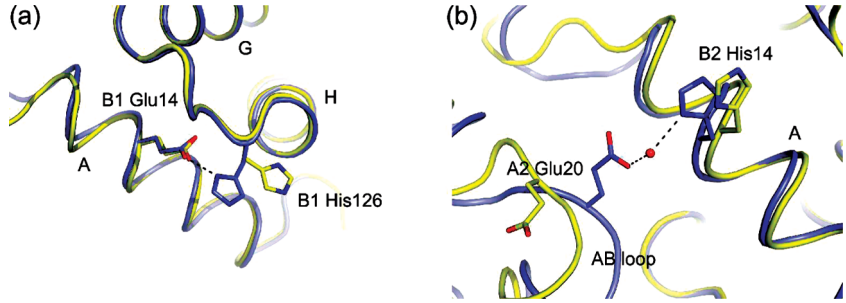


FIGURE 5: Suggested key residues involved in the Bohr effect. The structure of met(A1-oxy)Hb (blue) is superimposed onto that of Ca-oxyHb (yellow), which is representative of all oxygenated forms. Helical regions are indicated. (a) Rotamer rearrangement of His126 in the met(A1-oxy)Hb structure forms a salt bridge with the Glu14 residue in the B1 subunit. The structures were superimposed onto each of the B1 subunits with rms displacements of 1.3 Å (156 Cα atoms). (b) A large structural change in the AB loop of the A2 subunit results in rearrangement of the side chain of Glu20 toward B2 His14, which leads to the formation of a hydrogen bond network with a water molecule. The structures were superimposed onto each of the B2 subunits, with rms displacements of 1.0 Å (154 Cα atoms).

The evidence that has accumulated thus far suggests that $Ca^{2+}$ ions bind at site 2 and/or site 3 in the early steps of oxygenation, resulting in the left shift of the lower left end in the Hill plots, followed by binding at site 1 during the late steps of the reaction, leading to the left shift of the upper right end. Site 1 of Ca-oxyHb is identical to the $Mg^{2+}$-binding site of Mg-oxyHb and may have less affinity for metal ions than sites 2 and 3 have. The lower affinity for metal ions at site 1 in this molecule coincides with the shift of the upper right end in the Hill plots with the $Mg^{2+}$ condition. Site 4 might be only slightly, if at all, involved in the cooperativity, because this site is not observed to be involved in interactions between any subunits.

Sequence alignments and comparisons of the structures around the metal-binding sites in *Oligobrachia* Hb and the dodecamer subassembly of *Lumbricus* Hb have revealed that most of these sites are not conserved. The amino acid sequences at site 1 are not completely conserved between *Oligbrachia* and *Lumbricus* Hb. Site 2 is located at the interface between two dodecamer subassemblies that do not exist in *Lumbricus* Hb. Only at site 3 are two metal-coordinating aspartate residues conserved, and these residues are arranged in almost the same conformation in *Lumbricus* Hb ($P_{50}$ = 12.7 mmHg, and $n$ = 6.6 at pH 7.4 under no-metal conditions) (*15*), which indicates that in *Lumbricus* Hb, the $Ca^{2+}$ ion could also bind at this site. However, in the structure of the entire *Lumbricus* Hb molecule under crystallization conditions with 10 mM $CaCl_2$, no $Ca^{2+}$ ions were observed at either site 1 or site 3 of *Oligobrachia* Ca-oxyHb (*21*). The oxygen binding properties with the divalent cations of *Oligobrachia* Hb and those of *Lumbricus* Hb are qualitatively similar in terms of the left-shift properties of the Hill plots, but the metal-binding sites appear to differ to some extent.

While $Cl^-$ ions have not been reported to exert any influence on the oxygenation properties of *Oligobrachia* Hb (*19*) and *Lumbricus* Hb (*15*), $Cl^-$ density is clearly observed in both Ca- and Mg-oxyHb. Although the crystallization reagent and cryoprotectant solution contained approximately 60 mM $Cl^-$ in the Tris-HCl buffer used in a previously reported study of *Oligobrachia* oxyHb (*18*), no peaks for potential ions or water molecules were observed in the corresponding area, and the side chain of the A1 Arg4 residue was oriented away from the $Cl^-$ site. The structure of met(A1-oxy)Hb also lacked a $Cl^-$ site, as the crystal was soaked in cryoprotectant solution containing no $Cl^-$ ions (*24*). In contrast, the cryoprotectant solution used to determine the structures of Ca- and Mg-oxyHb contained ~160 mM $Cl^-$, which was derived from $CaCl_2$ or $MgCl_2$, and HCl (for pH adjustment). Higher concentrations of $Cl^-$ ions might lead to $Cl^-$ binding in Ca- and Mg-oxyHb structures.

Oxygenation property analysis using different pH values revealed a small Bohr coefficient (−0.28) of *Oligobrachia* Hb (*19*), which indicates that 0.28 proton per heme is released during the oxygenation reaction. Considering that the Bohr effect is observed at near-neutral pH, histidine side chains provide the most likely sites for proton binding, due to their p$K_a$ values. Comparisons of Ca- and Mg-oxyHb structures with that of met(A1-oxy)Hb suggest putative proton-binding sites on the histidine residues in the case of the Bohr effect in *Oligobrachia* Hb. In met(A1-oxy)Hb, the side chain of B1 His126 is directed toward B1 Glu14 and forms a salt bridge (Figure 5a). This tertiary rearrangement would cause an increase in the p$K_a$ of B1 His126 and would facilitate the protonation of this residue. Another candidate is His14 of the B2 subunit. In met(A1-oxy)Hb, A2 Glu20 is located near B2 His14, forming a hydrogen bond network via a water molecule (Figure 5b), while the electron densities around A2 Glu20 are found to be very weak in the metal-bound forms. The rearrangement of the acidic residue near B2 His14 would also increase the p$K_a$ of B2 His14. On the other hand, the mechanisms for Bohr effects of other annelids may be different from that of *Oligobrachia* Hb, discussed above. B1 His126 is not conserved in *Lumbricus* Hb. While B2 His14 is conserved, there is no acidic residue at the A2 Glu20 position. Other proton-binding sites may be included in the pH-dependent oxygenation properties of *Lumbricus* Hb. The higher Bohr coefficient of −0.61 (*15*) would indicate the existence of additional proton-binding sites.

*Homotropic Interaction.* The dimer subassembly (A1B1 and A2B2 dimers) in the 24-mer *Oligobrachia* Hb could play a primary role in homotropic cooperativity, because each heme directly interacts with the neighboring subunit in this dimer structure. Recent studies of mammalian tetrameric Hbs provide evidence of multiple R states (*8, 9*), and extended allostery models (*10*) have been proposed. We previously reported the quaternary changes between *Oligobrachia* oxyHb and met(A1-oxy)Hb of the dimer subassemblies (*24*). The structures of Ca- and Mg-oxyHb in this study are identical to that of metal-free oxyHb (*18*), indicating that this quaternary state may reveal one of the high-ligand affinity R states of the giant Hb. The high-resolution

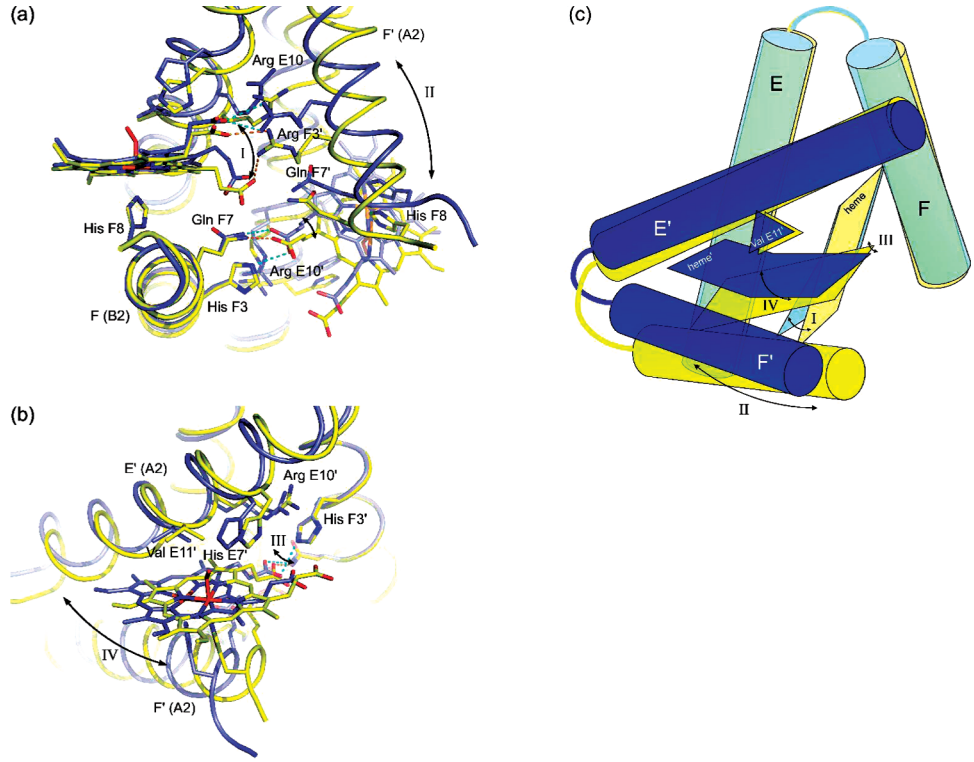


FIGURE 6: Ligand-induced structural changes around the interface region of the dimer subassembly. The structure of met(A1-oxy)Hb (blue) is superimposed onto the proximal histidine (F8) of Ca-oxyHb (yellow). The arrows indicate the relative scale of the structural movements. (a) View of the area around the A2B2 dimer interface region. Residues marked with a prime belong to the A2 subunit. (b) Another view of the area around the heme pocket of the A2 subunit. The larger movement of the F′ helix with respect to the E′ helix reflects the distances between each C$\beta$ atom of Val E11′ and the heme iron atom, i.e., 1.4 and 2.1 Å, respectively. The structural changes in the A1B1 dimer interface are essentially the same as those in the A2B2 dimer. (c) Schematic diagram of the quaternary transitions. The E and F helices and hemes of each subunit of the dimer subassembly are indicated. Val E11′, which is a key residue for the control of the environment of the heme pocket from the low-affinity closed form to the high-affinity open form, is also shown. The arrows and Roman numeral correspond to that of those of panels a and b.

structures of Ca- and Mg-oxyHb, together with that of met(A1-oxy)Hb, which could be very similar to one of the low-ligand affinity T states, provide insight into the mechanism of the homotropic cooperativity of *Oligobrachia* Hb.

The bent geometry of each of the hemes in partially unliganded met(A1-oxy)Hb is sifted to the planar geometry in the oxygenated Ca- and Mg-oxyHb structures (Figure S2 of the Supporting Information). Comparison of the dimer subassembly of Ca-oxyHb with that of met(A1-oxy)Hb (Figure 6a) reveals that the relaxation of the heme plane during the oxygenation step leads to the sliding of the neighboring F′ helix (the prime symbol indicates it belongs to the neighboring subunit). This sliding of the F′ helix would be caused by the interactions of propionate group of the heme with His (or Arg) F3′ and Gln F7′. The movement of the F′ helix includes movement of the coordinating heme′, and a rotation of 6−7° occurs at the Fe position (Figure 6b). In contrast, the E′ helix moves little, because the interactions of Arg E10′ with the F helix (the former subunit) prohibit a great deal of movement. The movements of the E′ and F′ helices result in the rearrangement of the relative positions between heme′ and Val E11′. Val E11′, which reduces the space of the distal pocket in the unliganded form (*24*), moves away from the heme pocket with the rotation of heme′, forming an open conformation that is favorable for binding of the ligand.

The ligand-induced rearrangement of the dimer structure of *Oligobrachia* Hb is quite different from that of HbI of *Scapharca inaequivalvis*, which assumes the same EF dimer structure (*13, 14*). The residues involved in the dimer interface region composed of the E and F helices are not conserved between *Oligobrachia* Hb and *Scapharca* HbI, and the ligand-induced heme movement of the *Scapharca* HbI is not a rotation, but rather a translation type of movement deeper into the prosthetic cavity (*35*). Among the 400 and 3600 kDa giant Hbs, all the key residues, Arg E10, His (Arg) F3, and Gln F7 at the interface of the dimer subassembly and Val E11 at the distal pocket, are highly conserved. The quaternary rotation mechanism of homotropic cooperativity might be shared among giant Hbs.

## ACKNOWLEDGMENT

We thank Dr. K. Imai for helpful discussions and Drs. K. Hasegawa, M. Kawamoto, H. Sakai, E. Yamashita, M. Yoshimura, T. Hikima, and Y. Kawano of SPring-8 for their help with the X-ray diffraction experiments.

## SUPPORTING INFORMATION AVAILABLE

Electron density maps around the ligand sites in all subunits in both Ca- and Mg-oxyHb (Figure S1) and heme geometry of all subunits in both Ca- and Mg-oxyHb compared with that in met(A1-oxy)Hb (Figure S2). This material is available free of charge via the Internet at http://pubs.acs.org.

## REFERENCES


1. Bohr, C., Hasselbach, K. A., and Krogh, A. (1904) Über einen in biologischen Beziehung wichtigen Einfluss, den die Kohlensauerspannung des Blutes auf dessen Sauerstoffbindung übt. *Skand. Arch. Physiol. 15*, 401–412.
2. Perutz, M. F. (1970) Stereochemistry of cooperative effects in haemoglobin. *Nature 228*, 726–739.
3. Monod, J., Wyman, J., and Changeux, J. P. (1965) On the nature of allosteric transitions: A plausible model. *J. Mol. Biol. 12*, 88–118.
4. Fronticelli, C., Bucci, E., and Razynska, A. (1988) Modulation of oxygen affinity in hemoglobin by solvent components. Interaction of bovine hemoglobin with 2,3-diphosphoglycerate and monatomic anions. *J. Mol. Biol. 202*, 343–348.
5. Kavanaugh, J. S., Rogers, P. H., Case, D. A., and Arnone, A. (1992) High-resolution X-ray study of deoxyhemoglobin Rothschild 37$\beta$ Trp → Arg: A mutation that creates an intersubunit chloride-binding site. *Biochemistry 31*, 4111–4121.
6. Perutz, M. F., Fermi, G., Poyart, C., Pagnier, J., and Kister, J. (1993) A novel allosteric mechanism in haemoglobin. Structure of bovine deoxyhaemoglobin, absence of specific chloride-binding sites and origin of the chloride-linked Bohr effect in bovine and human haemoglobin. *J. Mol. Biol. 233*, 536–545.
7. Rivetti, C., Mozzarelli, A., Rossi, G. L., Kwiatkowski, L. D., Wierzba, A. M., and Noble, R. W. (1993) Effect of chloride on oxygen binding to crystals of hemoglobin Rothschild ($\beta$37 Trp → Arg) in the T quaternary structure. *Biochemistry 32*, 6411–6418.
8. Shibayama, N., Miura, S., Tame, J. R., Yonetani, T., and Park, S. Y. (2002) Crystal structure of horse carbonmonoxyhemoglobin-bezafibrate complex at 1.55-Å resolution. A novel allosteric binding site in R-state hemoglobin. *J. Biol. Chem. 277*, 38791–38796.
9. Yokoyama, T., Neya, S., Tsuneshige, A., Yonetani, T., Park, S. Y., and Tame, J. R. (2006) R-state haemoglobin with low oxygen affinity: Crystal structures of deoxy human and carbonmonoxy horse haemoglobin bound to the effector molecule L35. *J. Mol. Biol. 356*, 790–801.
10. Yonetani, T., Park, S. I., Tsuneshige, A., Imai, K., and Kanaori, K. (2002) Global allostery model of hemoglobin. Modulation of $O_2$ affinity, cooperativity, and Bohr effect by heterotropic allosteric effectors. *J. Biol. Chem. 277*, 34508–34520.
11. Bolognesi, M., Bordo, D., Rizzi, M., Tarricone, C., and Ascenzi, P. (1997) Nonvertebrate hemoglobins: Structural bases for reactivity. *Prog. Biophys. Mol. Biol. 68*, 29–68.
12. Weber, R. E., and Vinogradov, S. N. (2001) Nonvertebrate hemoglobins: Functions and molecular adaptations. *Physiol. Rev. 81*, 569–628.
13. Royer, W. E., Jr., Knapp, J. E., Strand, K., and Heaslet, H. A. (2001) Cooperative hemoglobins: Conserved fold, diverse quaternary assemblies and allosteric mechanisms. *Trends Biochem. Sci. 26*, 297–304.
14. Royer, W. E., Jr., Zhu, H., Gorr, T. A., Flores, J. F., and Knapp, J. E. (2005) Allosteric hemoglobin assembly: Diversity and similarity. *J. Biol. Chem. 280*, 27477–27480.
15. Fushitani, K., Imai, K., and Riggs, A. F. (1986) Oxygenation properties of hemoglobin from the earthworm *Lumbricus terrestris*. Effects of pH, salts, and temperature. *J. Biol. Chem. 261*, 8414–8423.
16. Yuasa, H. J., Green, B. N., Takagi, T., Suzuki, N., Vinogradov, S. N., and Suzuki, T. (1996) Electrospray ionization mass spectrometric composition of the 400 kDa hemoglobin from the pogonophoran *Oligobrachia mashikoi* and the primary structures of three major globin chains. *Biochim. Biophys. Acta 1296*, 235–244.
17. Nakagawa, T., Onoda, S., Kanemori, M., Sasayama, Y., and Fukumori, Y. (2005) Purification, characterization and sequence analyses of the extracellular giant hemoglobin from *Oligobrachia mashikoi*. *Zool. Sci. 22*, 283–291.
18. Numoto, N., Nakagawa, T., Kita, A., Sasayama, Y., Fukumori, Y., and Miki, K. (2005) Structure of an extracellular giant hemoglobin of the gutless beard worm *Oligobrachia mashikoi*. *Proc. Natl. Acad. Sci. U.S.A. 102*, 14521–14526.
19. Aki, Y., Nakagawa, T., Nagai, M., Sasayama, Y., Fukumori, Y., and Imai, K. (2007) Oxygenation properties of extracellular giant hemoglobin from *Oligobrachia mashikoi*. *Biochem. Biophys. Res. Commun. 360*, 673–678.
20. Strand, K., Knapp, J. E., Bhyravbhatla, B., and Royer, W. E., Jr. (2004) Crystal structure of the hemoglobin dodecamer from *Lumbricus* erythrocruorin: Allosteric core of giant annelid respiratory complexes. *J. Mol. Biol. 344*, 119–134.
21. Royer, W. E., Jr., Sharma, H., Strand, K., Knapp, J. E., and Bhyravbhatla, B. (2006) Lumbricus erythrocruorin at 3.5 Å resolution: Architecture of a megadalton respiratory complex. *Structure 14*, 1167–1177.
22. Royer, W. E., Jr., Omartian, M. N., and Knapp, J. E. (2007) Low resolution crystal structure of *Arenicola erythrocruorin*: Influence of coiled coils on the architecture of a megadalton respiratory protein. *J. Mol. Biol. 365*, 226–236.
23. Flores, J. F., Fisher, C. R., Carney, S. L., Green, B. N., Freytag, J. K., Schaeffer, S. W., and Royer, W. E., Jr. (2005) Sulfide binding is mediated by zinc ions discovered in the crystal structure of a hydrothermal vent tubeworm hemoglobin. *Proc. Natl. Acad. Sci. U.S.A. 102*, 2713–2718.
24. Numoto, N., Nakagawa, T., Kita, A., Sasayama, Y., Fukumori, Y., and Miki, K. (2008) Structure of the partially unliganded met state of 400 kDa hemoglobin: Insights into ligand-induced structural changes of giant hemoglobins. *Proteins 73*, 113–125.
25. Sasayama, Y., Matada, M., Fukumori, Y., Umebayashi, M., Matsuno, A., Nakagawa, T., and Imajima, M. (2003) External morphology of the posterior end, the "opisthosoma", of the beard worm *Oligobrachia mashikoi* (Pogonophora). *Zool. Sci. 20*, 1411–1416.
26. Otwinowski, Z., and Minor, W. (1997) Processing of X-ray diffraction data collected in oscillation mode. *Methods Enzymol. 276*, 307–326.
27. Collaborative Computational Project, Number 4 (1994) The CCP4 suite: Programs for protein crystallography. *Acta Crystallogr. D50*, 760–763.
28. Vagin, A., and Teplyakov, A. (1997) MOLREP: An Automated Program for Molecular Replacement. *J. Appl. Crystallogr. 30*, 1022–1025.
29. Emsley, P., and Cowtan, K. (2004) Coot: Model-building tools for molecular graphics. *Acta Crystallogr. D60*, 2126–2132.
30. Murshudov, G. N., Vagin, A. A., and Dodson, E. J. (1997) Refinement of macromolecular structures by the maximum-likelihood method. *Acta Crystallogr. D53*, 240–255.
31. Brünger, A. T., Adams, P. D., Clore, G. M., DeLano, W. L., Gros, P., Grosse-Kunstleve, R. W., Jiang, J. S., Kuszewski, J., Nilges, M., Pannu, N. S., Read, R. J., Rice, L. M., Simonson, T., and Warren, G. L. (1998) Crystallography & NMR system: A new software suite for macromolecular structure determination. *Acta Crystallogr. D54*, 905–921.
32. Harding, M. M. (2006) Small revisions to predicted distances around metal sites in proteins. *Acta Crystallogr. D62*, 678–682.
33. Park, S. Y., Yokoyama, T., Shibayama, N., Shiro, Y., and Tame, J. R. (2006) 1.25 Å resolution crystal structures of human haemoglobin in the oxy, deoxy and carbonmonoxy forms. *J. Mol. Biol. 360*, 690–701.
34. Bogin, O., Kvansakul, M., Rom, E., Singer, J., Yayon, A., and Hohenester, E. (2002) Insight into Schmid metaphyseal chondrodysplasia from the crystal structure of the collagen X NC1 domain trimer. *Structure 10*, 165–173.
35. Knapp, J. E., Gibson, Q. H., Cushing, L., and Royer, W. E., Jr. (2001) Restricting the ligand-linked heme movement in *Scapharca* dimeric hemoglobin reveals tight coupling between distal and proximal contributions to cooperativity. *Biochemistry 40*, 14795–14805.


BI8012609